Nanoscale

Accepted Manuscript

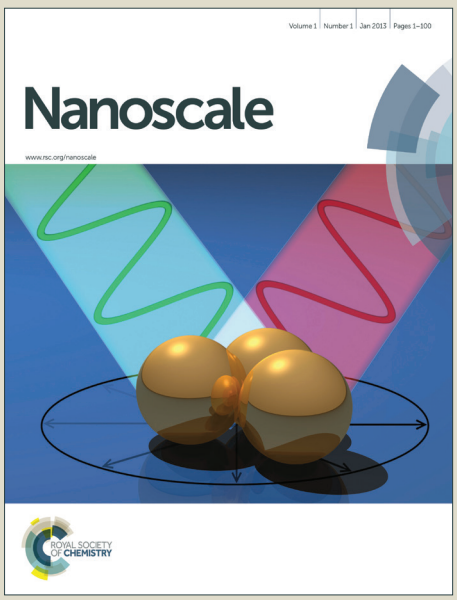

ROYAL SOCIETY OF CHEMISTRY

www.rsc.org/nanoscale

Probing the nature and resistance of the molecule-electrode contact in SAM-based junctions

C. S. Suchand Sangeeth,[1] Albert Wan,[1] and Christian A. Nijhuis[1,2]*

[1] Department of Chemistry, National University of Singapore, 3 Science Drive 3, Singapore 117543.

[2] Centre for Advanced 2D Materials and Graphene Research Centre, 6 Science Drive 2, Singapore 117546, Singapore.

Corresponding author:

Tel: +65 6516 2667

Fax: +65 6779 1691

e-mail: chmnca@nus.edu.sg

Abstract: It is challenging to quantify the contact resistance and to determine the nature of the molecule–electrode contacts in molecular two-terminal junctions. Here we show that potentiodynamic and temperature dependent impedance measurements give insight into the nature of the SAM–electrode interface and other bottlenecks of charge transport (the capacitance of the SAM (C_{SAM}) and resistance of the SAM (R_{SAM})), unlike DC methods, independently from each other. We found that the resistance of the top-electrode–SAM contact for junctions of the form of Ag^{TS}–SC_n//GaO_x/EGaIn with n = 10, 12, 14, 16 or 18, is bias and temperature independent and hence Ohmic (non-rectifying) in nature, and is orders of magnitude smaller than the resistance of the SAM (R_{SAM}). The capacitance of the SAM (C_{SAM}) and R_{SAM} are independent of the temperature, indicating

that the mechanism of charge transport in these SAM-based junctions is coherent tunneling and the charge carrier trapping at the interfaces is negligible.

Keywords: self-assembled monolayer, impedance spectroscopy, EGaIn junction, Ohmic contact, molecular electronics.

Introduction

Molecular junctions of the form of electrode–SAM–electrode (SAM = self-assembled monolayer) are appealing because of their potential of inducing, and controlling, electronic function at the nanometer length scales.[1-4] Understanding the nature of the molecule-electrode contacts in these two-terminal junctions is crucial in the interpretation of the data they generate. The strength of the molecule-electrode contact (e.g., covalent vs. non-covalent) determines how the molecular energy levels are coupled to the electrodes, the contact resistance affects the potential drop across the molecules, and some types of contacts (e.g., a Schottky contact) may dominate and mask the molecular properties of the junction.[4-6] Data generated by junctions with a protective barrier, which is usually inserted between the SAM and the top-electrode to prevent damage to the SAMs during fabrication of the top-electrode, greatly complicates the interpretation of the electrical characteristics.[1, 7-12] In general, low resistance and temperature-independent Ohmic molecule-electrode contacts are desirable to ensure that molecular effects dominate the electrical characteristics of the junction.[9, 13-16] However, the nature of the molecule-electrode contact, and how it depends on the applied bias and temperature, is unknown for most two-terminal SAM-based molecular junctions.[9, 11, 17, 18] Therefore, a method to measure the properties of the molecule-electrode contact along with the other components of the junction that impede charge transport independently from each other is needed.

The electrical properties of electrode–SAM–electrode junctions are usually studied by two-terminal DC measurements.[1, 17] These measurements only determine the total current (impeded by all components of the junction) that flows across a junction as a function of

applied bias and do not distinguish the contributions of each component (the SAM, the electrodes, and the two SAM–electrode interfaces) to the measured current complicating the interpretation of these data.[17] For reasons of simplicity, the DC data (more specifically *J*(V) data) are often interpreted using the general tunneling equation (eqn (1)) where β is the tunneling decay constant (in n_C^{-1}), d_{SAM} is the thickness of the SAM (in n_C), and J_0 is the hypothetical current through the junction for d_{SAM} = 0 n_C.[19] The values of β and J_0 are determined from plots of *J* (at a given V) vs. *d* by extrapolation of the data to *d* = 0 n. Since eqn (1) is only valid at very low applied bias (i.e., around 0 V) this method does not reveal the nature of the metal—molecule contact directly and the interpretation of the value of J_0 (which is usually related to the SAM—electrode properties) relies on many assumptions.[20]

$$J = J_0 e^{-\beta d_{SAM}} \quad (1)$$

To investigate the effect of the SAM–metal contact on the electronic transport characteristics in more detail, Lee *et al.* extended the Simmons equation and proposed a multi barrier tunneling model in which the junction is divided into three tunnel barriers posed by the SAM and the two molecule–metal contacts (see below).[21] This method still relies on long extrapolations and fitting of *J*(V) data using a large number of fitting parameters. Recently we showed that impedance spectroscopy (an AC technique) makes it possible to isolate the contribution of each component in the junctions with the form of Ag^{TS}–SAM//GaO_x/EGaIn (Fig. 1) to the total impedance (where "–" indicates a chemical bond and "//" a non-covalent interface).[17] These measurements were only conducted at zero DC bias at 298 K and the results did not reveal the nature of the SAM//GaO_x/EGaIn

contact or how the individual circuit components respond to the applied bias or changes in temperature.[17]

Here we used temperature dependent and potentiodynamic impedance spectroscopy to study each component of the junction that impedes charge transport independently from each other and to determine how they depend on the applied bias (±0.50 V) and temperature (220 – 340 K). We studied junctions of Ag^{TS}–SC_n//GaO_x/EGaIn with n = 10, 12, 14, 16 or 18, because these junctions can be formed in high yields of non-shorting junctions in statistically large numbers under ordinary laboratory conditions (e.g., clean rooms are not required).[7, 17, 19, 22, 23] In these junctions (Fig. 1), the native 0.7 nm thick layer of GaO_x is a protective barrier that prevents the bulk EGaIn from alloying with the bottom-electrode.[7, 12] Previous studies showed that the GaO_x layer is highly conductive,[7, 12, 17, 19] but the nature of the SAM//top-electrode interface and how it affects the electrical properties of the junctions remain unclear. In the case of an Ohmic contact, the injection rate of charge carriers depends on the contact resistance and is independent on the applied voltage or temperature.[24] On the other hand, the resistance of a Schottky contact, for instance, depends on the Schottky barrier height which is influenced by both the applied voltage and temperature.[24] In this article we show that temperature dependent and potentiodynamic impedance spectroscopy makes it possible to study the nature of the SAM//GaO_x contact and that it is independent of the applied bias or temperature from which we conclude that it behaves as an Ohmic. In addition, the SAM//GaO_x contact resistance is more than 4 orders of magnitude lower than the resistance of the SAMs. We believe that this method to determine the nature of the SAM–electrode contact in two-terminal SAM-based junctions can also be applied to other systems.

Experimental

We used GaO_x/EGaIn top-electrode stabilized in a through-hole made in a transparent rubber of polydimethylsiloxane (PDMS) following previously reported methods.[22] These junctions are stable against bias stressing and temperature changes, and have well-defined geometrical contact areas (A_{geo}).[22] In this study, A_{geo} was 9.6×10^2 μm^2 in all of our measurements. The preparation of the template-stripped Ag bottom electrode, the SAMs, and the junctions, have been reported in detail elsewhere (see Supporting Information for more details).[22, 25] In our studies, we only used junctions that had values of $\log_{10}|J|$ within one log-standard deviation of the Gaussian mean value of $\log_{10}|J|$ (i.e., $<\log_{10}|J|>_G$) which are reported in reference 22. The J(V) measurements were carried out using a keithley 6430 source meter and data were acquired using LabView 2010. The frequency dependent impedance measurements were carried out using a Solartron impedance analyzer (model 1260A with 1296A dielectric interface) by superimposing the sinusoidal perturbation (ranging from 1 Hz to 1 MHz with 12 frequencies per decade) on the desired DC bias ranging from -0.50 V to 0.50 V in steps of 0.10 V with an amplitude of 20 mV for junctions with n = 10 or 12, and 30 mV for junctions with n = 14, 16, or 18 (to improve the signal-to-noise ratio). The temperature dependent impedance measurements were performed in a probe station (Lakeshore CRX-VF) at a pressure of 3×10^{-5} bar.

Results and discussion

Figure 1 shows a schematic illustration of the Ag^{TS}–SC_n//GaO_x/EGaIn junction and the equivalent circuit we used to fit the experimental data. The impedance data show that

these junctions can be modeled with an equivalent circuit consisting of the resistance of the SAM (R_{SAM} in $\Omega \cdot cm^2$) in parallel with the capacitance of the SAM (C_{SAM} in $\mu F/cm^2$), both in series with the contact resistance (R_C in $\Omega \cdot cm^2$). Below we give a physical interpretation of each circuit element, but first we describe the equivalent circuit. The resistance of the 0.7 nm thick GaO_x protective layer is $3.3 - 5.8 \times 10^{-4}$ $\Omega \cdot cm^2$ and has a negligible effect on the charge transport properties in DC measurements.[12, 17] We showed before that R_C is dominated by the resistance of the non-covalent SAM//top-electrode interface ($R_{C,t}$ where t denotes the top-contact) and that the contributions from the resistances of the wires, contact probes, GaO_x layer, and the covalent Ag^{TS}–S interface ($R_{C,b}$ where b denotes the bottom-contact) are minor.[17] Thus, the assumption that $R_C = R_{C,t}$, where t denotes top-contact (Fig. 1), only introduces a small error (~ 2%). This assumption agrees with the results reported by Whitesides *et al.* who showed that the observed tunneling rates across EGaIn junctions is independent of the nature of the bottom electrode—SAM for junctions (with Ag and Au bottom-electrodes with SAMs bound via acetylene, carboxylate, or thiolate anchoring groups).[26, 27] Figure 2 shows the J(V) data (the arithmetic mean of ten J(V) curves; the error bars represent the standard deviations) of the junctions we used here to determine the impedance spectra. The inset in Fig. 2a shows that a fit of the values of J determined at -0.50 V as a function of n_C to eqn (1) yields $\beta = 0.97 \pm 0.05$ n_C^{-1} and $J_0 = 247 \pm 5$ A/cm^2 (the errors represent the 95% confidence levels) which are indistinguishable from previously reported data.[22]

Figure 3a shows the Nyquist plots recorded across a junction with a SAM of SC_{10} determined over the range of DC biases of -0.5 V to 0.5 V in steps of 0.1 V (see Supporting Information for all other data obtained for the other junctions and the Bode

plots). Each Nyquist plot is the average of five measurements to improve the signal-to-noise ratios. We repeated this procedure three times with different junctions and the error bars in Fig. 3 represent the standard deviation of these three measurements. Before we analyzed the data, it is important to verify that the junctions were stable (in thermodynamic equilibrium) and that the data are linear (no harmonics are present).[28, 29] The data are Kramers-Kronig transformable with χ^2_{KK} in the range of $1\times10^{-3} - 1.5\times10^{-3}$ and the residual plots (Fig. S4 and S5) show that indeed that the 20 or 30 mV perturbation was small enough to ensure linear behavior. The residual plots of the fits show that the model fitted the experimental data well with χ^2_{fit} values similar to the χ^2_{KK} values (Table S1 and S2).

We used the following equivalent circuit to analyze all impedance data. The complex impedance Z is more general than the resistance as it also accounts for the phase and amplitude of the current in AC measurements (See Supporting Information). Here we modeled the junctions as a dielectric (i.e., the SAM) placed between two parallel plates (i.e., electrodes; Fig. 1b). The SAM offers impedance which is a parallel combination of R_{SAM} and C_{SAM} to the AC current flowing through the junction. The C_{SAM} itself gives rise to a resistance equal to the capacitive reactance ($X_c = 1/\omega C_{SAM}$; where ω (rad/s) is the frequency of the AC signal) that decreases with increasing frequency. The resistance of the contacts is modeled by a resistor in series R_C. For the equivalent circuit shown in Fig. 1b, the complex impedance Z is given by eqn (2)(See Supporting Information).[17]

$$Z = \left(R_C + \frac{R_{SAM}}{1+\omega^2 R_{SAM}^2 C_{SAM}^2} \right) - j\left(\frac{\omega C_{SAM} R_{SAM}^2}{1+\omega^2 R_{SAM}^2 C_{SAM}^2} \right) \qquad (2)$$

In Nyquist plots the imaginary component of Z is plotted against the real part and in Bode plots the value of modulus of complex impedance ($|Z|$) is plotted against the frequency (Fig. S2), we also show the phase ϕ (in °) against the frequency in Fig. S2 (for capacitors ϕ is 90° while for ideal resistors ϕ is 0°). Figure 3a shows that the impedance decreases with increasing DC bias in agreement with the DC measurements (Fig. 2).[30, 31] The Bode plots (Fig. S2) show that $|Z|$ is nearly constant at low frequencies (with ϕ is nearly 0°) and is dominated by R_{SAM}, but $|Z|$ decreases with increasing frequency due to the capacitive reactance (X_c) of the SAM. A capacitor appears as a semi-circle in the Nyquist plot and has a phase change of 90° (see Fig. S2) at high frequencies.[17, 28] The Nyquist plots only show one semi-circle which we attribute to C_{SAM}. At low frequencies, the spectra are dominated by R_{SAM} which has a 0° phase change (Fig. S2).[17]

To discuss the physical meaning of the elements of the equivalent circuit, we interpret the results in the frame work of the Landauer tunneling model which was modified to include the contact resistance associated with the coupling of the molecules to electrodes (eqn (3)) where h is the Planck's constant, e is the charge of an electron, T is the transmission probability, and M is the number of conduction channels.[32] In case of an ideal point contact, the contact resistance is the inverse of the universal quantum conductance $G_0 = 2e^2/h$ (for $M = 1$). From the Landauer theory eqn (1) can be derived because $T \propto e^{-\beta d}$.

$$R_{\text{junction}} = G_{\text{junction}}^{-1} = \frac{h}{2e^2M}\frac{1}{T} = \frac{h}{2e^2M} + \frac{h}{2e^2M}\frac{1-T}{T} = G_C^{-1} + G_{SAM}^{-1} = R_C + R_{SAM} \qquad (3)$$

To determine R_{SAM}, $R_{C,t}$, and C_{SAM}, we fitted the data using the equivalent circuit shown in Fig. 1b, and the solid lines in Fig. 3a are fits of the data to eqn (2). The voltage

dependence of the equivalent circuit components R_{SAM} and $R_{C,t}$ (=R_C) are shown in Fig. 3b and c, respectively. The value of R_{SAM} decreases exponentially with increasing bias in the high bias regime as expected for a tunneling process (see below and Fig. 3b).[17, 30, 31] In contrast, $R_{C,t}$ is constant over the applied range of biases, which indicates that the SAM//top electrode interface resembles Ohmic behavior. Thus the insignificant variation of R_C as a function of the molecular chain length and applied bias is in agreement with eqn (3).

Since surface coverage of the SAMs (4.5×10^{14} molecules/cm^2)[33] and the effective electrical contact area A_{elec} (which is 10^{-4} times the geometrical contact area A_{geo})[12] are known, we can determine the resistance per molecule in our junctions from R_{SAM}. We found the value of R_{SAM} lies in the range of single-molecule resistances[17] determined experimentally using scanning tunneling microscopy (STM) break-junctions[34, 35] and junctions based on conductive probe atomic force microscopy (Fig. S6).[18] For the contact resistance we obtain a value of 8.2×10^3 G_0^{-1} which is close (within 1 order of magnitude) to single molecule experiments involving junctions with one chemisorbed and one physisorbed contact as is the case in our EGaIn junctions. This is higher than the ideal contact resistance likely because of the presence of GaO_x layer which may not be an ideal reflectionless contact, or an underestimation of the correction factor for A_{elec}.

We validated the equivalent circuit by comparing the calculated currents from the AC measurements to that obtained by DC measurements, and by the analysis of R_{SAM} and C_{SAM}. Since the potentiodynamic impedance were measured by applying a small AC signal (ΔV) superimposed on a DC bias voltage while measuring the current response (ΔJ), the AC data are essentially the differential resistance of the junction ($\Delta V/\Delta J$) at that

DC bias voltage.[28, 36] Hence, the J(V) characteristics can be obtained by integrating the reciprocal of the impedance (= $\Delta J/\Delta V$) value over the applied DC bias voltage. Figure 2 shows that indeed that the J(V) characteristics obtained via potentiodynamic impedance spectroscopy and DC measurements are the same within error and indicates the consistency of measurements.

Equation 1 can be modified into eqn (4) to relate d_{SAM} to R_{SAM} where $R_{SAM,0}$ is the hypothetical resistance across the junction for d_{SAM} = 0 nm. A fit to R_{SAM} (determined at a DC bias of -0.50 V) as a function of n_C (inset of Fig. 2b) gives a value of β = 1.03 ± 0.05 n_C^{-1} and $R_{SAM,0}$ = 2.6 ± 0.4 ×10^{-4} Ω·cm^2 (the error represents the 95% confidence levels).[17] The value of β is within error of that obtained with DC measurements (Fig. 2a) which further confirms the validity of the equivalent circuit shown in Fig. 1b. The value $R_{SAM,0}$ is reasonably close to the $R_{C,t}$ value (which was on average 5.1 ± 1.2 ×10^{-3} Ω·cm^2) despite the very long extrapolation to d = 0 n_C (eqn (4)) which justifies the use of the simple framework to interpret the equivalent circuit. The observation that $R_{C,t}$ is constant as a function of d_{SAM} confirms that indeed in our experiments the details of the SAM—top contact were unchanged.

$$R_{SAM} = R_{SAM,0} e^{\beta d_{SAM}} \quad (4)$$

The inset of Fig. 3c shows the linear dependence of C_{SAM} as a function of $1/d_{SAM}$ as expected for a parallel plate capacitor described by eqn (5) where ε_0 is the permittivity of the free space and $\varepsilon_{r,SAM}$ is the dielectric constant of the SAM.[17, 36] Fitting these data to eqn (5) gave a value of $\varepsilon_{r,SAM}$ of 3.2 ± 0.2 which falls in the range of previously reported values.[17, 36, 37]

$$C_{SAM} = \varepsilon_0 \varepsilon_{r,SAM} A_{geo} / d_{SAM} \quad (5)$$

Figure 3d shows that C_{SAM} is independent of the applied voltage which proves that charge trapping at the molecule-electrode interface, or in the GaO_x layer, is not important.[24] This observation is in agreement with the lack of hysteresis in J(V) indicating that charging and discharging is insignificant. We showed before that the GaO_x layer can be modeled as a parallel RC circuit.[17] Here the native GaO_x layer is highly conductive, and the capacitance of the GaO_x layer has negligible contribution in the total impedance in the 1 Hz – 1 MHz frequency range. Therefore we conclude that the C_{SAM} is free of the contribution from the capacitance of GaO_x and is determined by the dielectric properties of the SAM.

To investigate how each circuit component depends on the temperature T (in K), we performed impedance spectroscopy at zero applied DC bias over the range of temperatures of 220 – 340 K at intervals of 10 K. Figure 4a shows that the Nyquist plots for a junction with a SC_{12} SAM are indistinguishable over the investigated range of temperatures (the temperature dependent impedance data for the other junctions with n = 10, 14, 16, and 18 are given in Fig. S7). From these data we obtained the values of R_{SAM}, C_{SAM}, and R_C, as a function of temperature. Figure 4b and 4c show that R_{SAM}, R_C and C_{SAM}, are independent of temperature which confirms that the mechanism of charge transport across the junctions is coherent through-bond tunneling. In addition, the observation that C_{SAM} does not vary with T confirms that no significant numbers of charge traps are present in our junctions (in case charge carrier traps would be important we would expect a decrease of the value of C_{SAM} with decreasing T).[24] Remarkably, the value of R_C is also independent of T which further proves that the GaO_x//SAM contacts behave as if they were Ohmic in nature.

Conclusions

In summary, we showed that temperature dependent and potentiodynamic impedance spectroscopy make it possible to elucidate the bias and temperature dependency of each circuit component of two-terminal SAM-based junctions, unlike DC measurements, independently from each other. This method allowed us to demonstrate that GaO_x/EGaIn top-electrodes form Ohmic contacts with low resistance to SAMs of n-alkanethiolates. Equally important, the capacitance of the junction is determined by the properties of the SAMs and is also independent of the applied bias or temperature, or the protective layer (here the GaO_x layer). Thus, over the entire range of applied biases and temperatures, we did not observe significant charge trapping (neither at the SAM–electrode interfaces nor in the GaO_x layer) or changes in the nature of the SAM–electrode contacts. The resistance of the SAM is independent of temperature and decreases exponentially with increasing applied bias. Based on these observations we conclude that the mechanism of charge transport across the junctions is coherent tunneling.

We believe that impedance spectroscopy as a function of temperature and applied DC bias is a useful and complementary tool to DC measurements to elucidate how each component of two-terminal SAM-based junctions impedes charge transfer which is important to know in establishing the mechanism of charge transport. In addition, this technique can potentially be useful to characterize other types of junctions with, for instance, redox-active SAMs or layers of biomolecules.

Acknowledgements

This research is supported by the National Research Foundation, Prime Minister's Office, Singapore under its medium sized centre program. The Singapore National Research Foundation (NRF Award No. NRF-RF 2010-03 to C.A.N.) is also gratefully acknowledged for supporting this research.

Supporting information

Electronic supplementary information (ESI) available: Detailed experimental procedure, Nyquist plots, summary of Krammers-Kronig and residual analysis, single molecule resistance plot.

Notes and references

1. Akkerman, H. B.; de Boer, B., *J. Phys.: Condens. Matter* 2008, **20,** 1-20.
2. McCreery, R. L.; Bergren, A. J., *Adv. Mater.* 2009, **21,** 4303-4322.
3. Tan, S. F.; Wu, L.; Yang, J. K. W.; Bai, P.; Bosman, M.; Nijhuis, C. A., *Science* 2014, **343,** 1496-1499.
4. Haick, H.; Cahen, D., *Prog. Surf. Sci.* 2008, **83,** 217-261.
5. Moth-Poulsen, K.; Bjørnholm, T., *Nat. Nanotechnol.* 2009, **4,** 551-556.
6. Lindsay, S. M.; Ratner, M. A., *Adv. Mater.* 2007, **19,** 23-31.
7. Nijhuis, C. A.; Reus, W. F.; Whitesides, G. M., *J. Am. Chem. Soc.* 2009, **131,** 17814-17827.
8. Neuhausen, A. B.; Hosseini, A.; Sulpizio, J. A.; Chidsey, C. E. D.; Goldhaber-Gordon, D., *ACS Nano* 2012, **6,** 9920-9931.
9. Wimbush, K. S.; Fratila, R. M.; Wang, D.; Qi, D.; Liang, C.; Yuan, L.; Yakovlev, N.; Loh, K. P.; Reinhoudt, D. N.; Velders, A. H.; Nijhuis, C. A., *Nanoscale* 2014, **6,** 11246-11258.
10. Bowers, C. M.; Liao, K.-C.; Yoon, H. J.; Rappoport, D.; Baghbanzadeh, M.; Simeone, F. C.; Whitesides, G. M., *Nano Lett.* 2014, **14,** 3521-3526.
11. Ricœur, G.; Lenfant, S.; Guérin, D.; Vuillaume, D., *J. Phys. Chem. C* 2012, **116,** 20722-20730.
12. Simeone, F. C.; Yoon, H. J.; Thuo, M. M.; Barber, J. R.; Smith, B.; Whitesides, G. M., *J. Am. Chem. Soc.* 2013, **135,** 18131-18144.
13. Heimel, G.; Romaner, L.; Zojer, E.; Bredas, J.-L., *Acc. Chem. Res.* 2008, **41,** 721-729.
14. Salomon, A.; Böcking, T.; Gooding, J. J.; Cahen, D., *Nano Lett.* 2006, **6,** 2873-2876.

15. Aradhya, S. V.; Venkataraman, L., *Nat. Nanotechnol.* 2013, **8,** 399-410.
16. Yuan, L.; Nerngchamnong, N.; Liang, C.; Hamoudi, H.; del Barco, E.; Roemer, M.; Sriramula, R. K.; Thompson, D.; Nijhuis, C. A., *Nat. Commun.* 2015, **6,** 6324.
17. Sangeeth, C. S. S.; Wan, A.; Nijhuis, C. A., *J. Am. Chem. Soc.* 2014, **136,** 11134-11144.
18. Engelkes, V. B.; Beebe, J. M.; Frisbie, C. D., *J. Am. Chem. Soc.* 2004, **126,** 14287-14296.
19. Nijhuis, C. A.; Reus, W. F.; Barber, J. R.; Whitesides, G. M., *J. Phys. Chem. C* 2012, **116,** 14139-14150.
20. Jiang, L.; Sangeeth, C. S. S.; Wan, A.; Vilan, A.; Nijhuis, C. A., *J. Phys. Chem. C* 2015, **119,** 960-969.
21. Wang, G.; Kim, T.-W.; Lee, H.; Lee, T., *Phys. Rev. B* 2007, **76,** 205320.
22. Wan, A.; Jiang, L.; Sangeeth, C. S. S.; Nijhuis, C. A., *Adv. Fun. Mater.* 2014, **24,** 4442-4456.
23. Nerngchamnong, N.; Yuan, L.; Qi, D.-C.; Li, J.; Thompson, D.; Nijhuis, C. A., *Nat. Nanotechnol.* 2013, **8,** 113-118.
24. Sze, S. M.; Nag, K. K., *Physics of Semiconductor Devices, 3rd ed.* Wiley: New York, 2007.
25. Yuan, L.; Jiang, L.; Zhang, B.; Nijhuis, C. A., *Angew. Chem., Int. Ed.* 2014, **53,** 3377-3381.
26. Yoon, H. J.; Shapiro, N. D.; Park, K. M.; Thuo, M. M.; Soh, S.; Whitesides, G. M., *Angew. Chem. Int. Ed.* 2012, **51,** 4658-4661.
27. Bowers, C. M.; Liao, K.-C.; Zaba, T.; Rappoport, D.; Baghbanzadeh, M.; Breiten, B.; Krzykawska, A.; Cyganik, P.; Whitesides, G. M., *ACS Nano* 2015, **9,** 1471-1477.
28. Macdonald, J. R.; Johnson, W. B., Fundamentals of Impedance Spectroscopy. In *Impedance Spectroscopy*, John Wiley & Sons, Inc.: 2005; pp 1-26.
29. Boukamp, B. A., *Solid State Ionics* 1986, **20,** 31-44.
30. Cuevas, J. C.; Scheer, E., *Molecular Electronics: An Introduction to Theory and Experiment*. World Scientific: Singapore: 2010.
31. McCreery, R. L.; Wu, J.; Prasad Kalakodimi, R., *Phys. Chem. Chem. Phys.* 2006, **8,** 2572-2590.
32. Datta, S., *Electronic transport in mesoscopic systems*. Cambridge university press: Cambridge, UK, 1995.
33. Love, J. C.; Estroff, L. A.; Kriebel, J. K.; Nuzzo, R. G.; Whitesides, G. M., *Chem. Rev.* 2005, **105,** 1103-1169.
34. Chen, F.; Li, X.; Hihath, J.; Huang, Z.; Tao, N., *J. Am. Chem. Soc.* 2006, **128,** 15874.
35. Li, C.; Pobelov, I.; Wandlowski, T.; Bagrets, A.; Arnold, A.; Evers, F., *J. Am. Chem. Soc.* 2008, **130,** 318.
36. Akkerman, H. B.; Naber, R. C. G.; Jongbloed, B.; van Hal, P. A.; Blom, P. W. M.; de Leeuw, D. M.; de Boer, B., *Proc. Natl. Acad. Sci.* 2007, **104,** 11161-11166.
37. Rampi, M. A.; Schueller, O. J. A.; Whitesides, G. M., *Appl. Phys. Lett.* 1998, **72,** 1781-1783.

Figures:

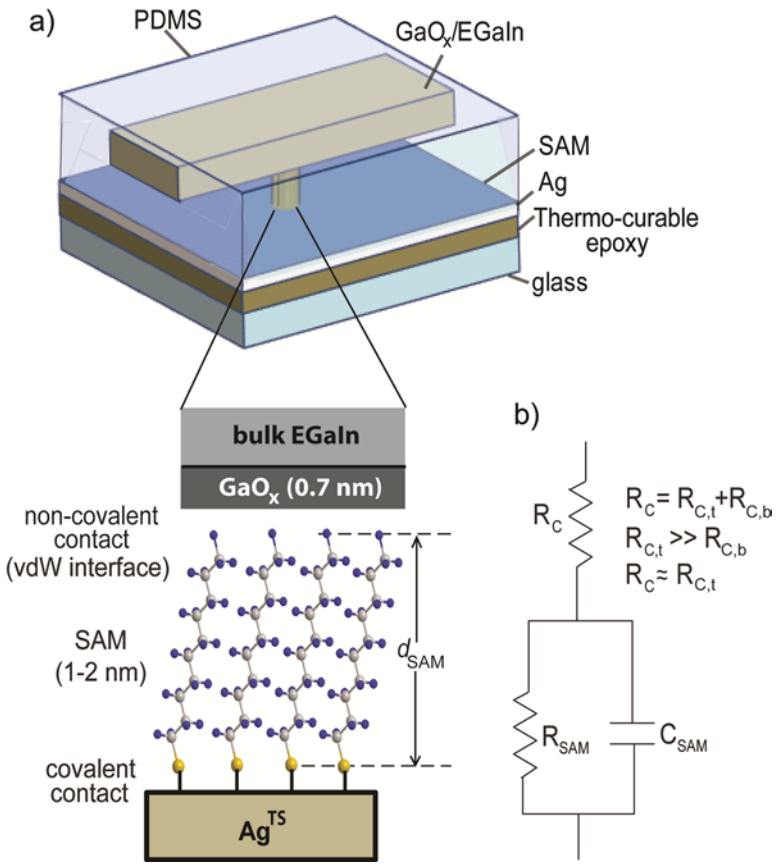

Figure 1: a) Schematic illustration of the SAM-based junctions with vdW = van der Waals interface (not drawn to scale). The liquid-metal GaO_x/EGaIn top electrode is encapsulated by the insulating polydimethylsiloxane (PDMS) and the Ag bottom electrode. EGaIn = eutectic Ga and In alloy, GaO_x = 0.7 nm thick conductive oxide consisting or predominantly Ga_2O_3, Ag^{TS} = template-stripped Ag surface. b) The equivalent circuit for the junctions that was used in the analysis of the impedance data. $R_{C,t}$ = the resistance of the SAM−top electrode interface and $R_{C,b}$ = the resistance of the SAM−bottom electrode interface. The resistance R_C is dominated by the non-covalent GaO_x//SAM contact.

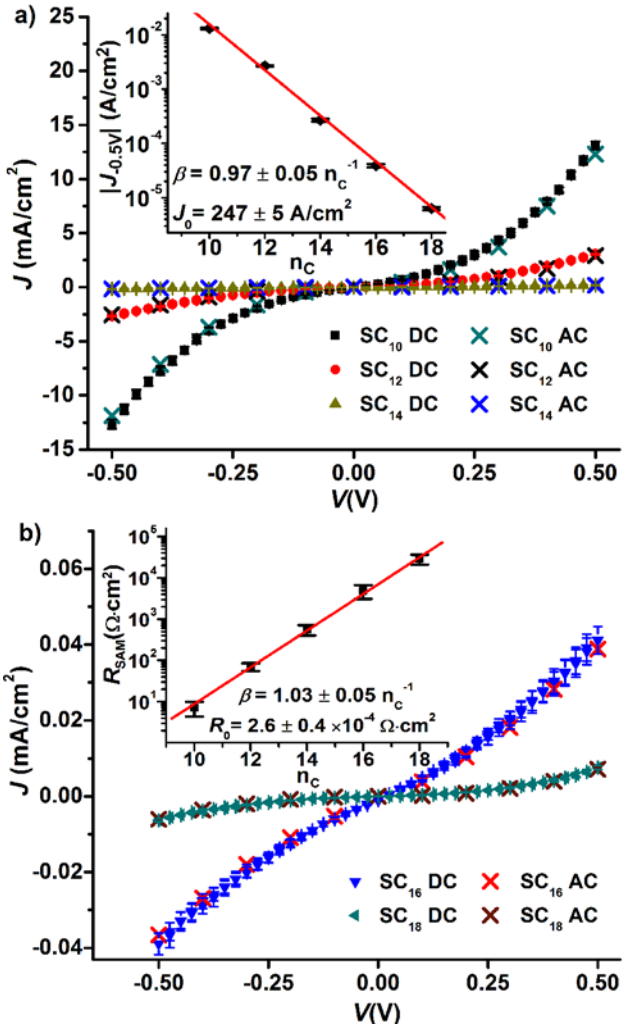

Figure 2: a) The average *J*(V) traces (one trace ≡ 0 V → 0.50 V → -0.50 V → 0 V) of the Ag^{TS}–SC_n//GaO_x/EGaIn junctions (with n = 10, 12, and 14) and the *J*(V) curves estimated from the impedance data, and b) the same for junctions with n = 16 and 18. The inset of panel a shows the value of |*J*| as a function of n_C measured at -0.50 V and the solid red line is a fit to eqn (1). The inset of panel b shows the R_{SAM} vs. n_C (determined by impedance spectroscopy at a DC bias of -0.50 V) with a fit to eqn (4). The error bars are standard deviations.

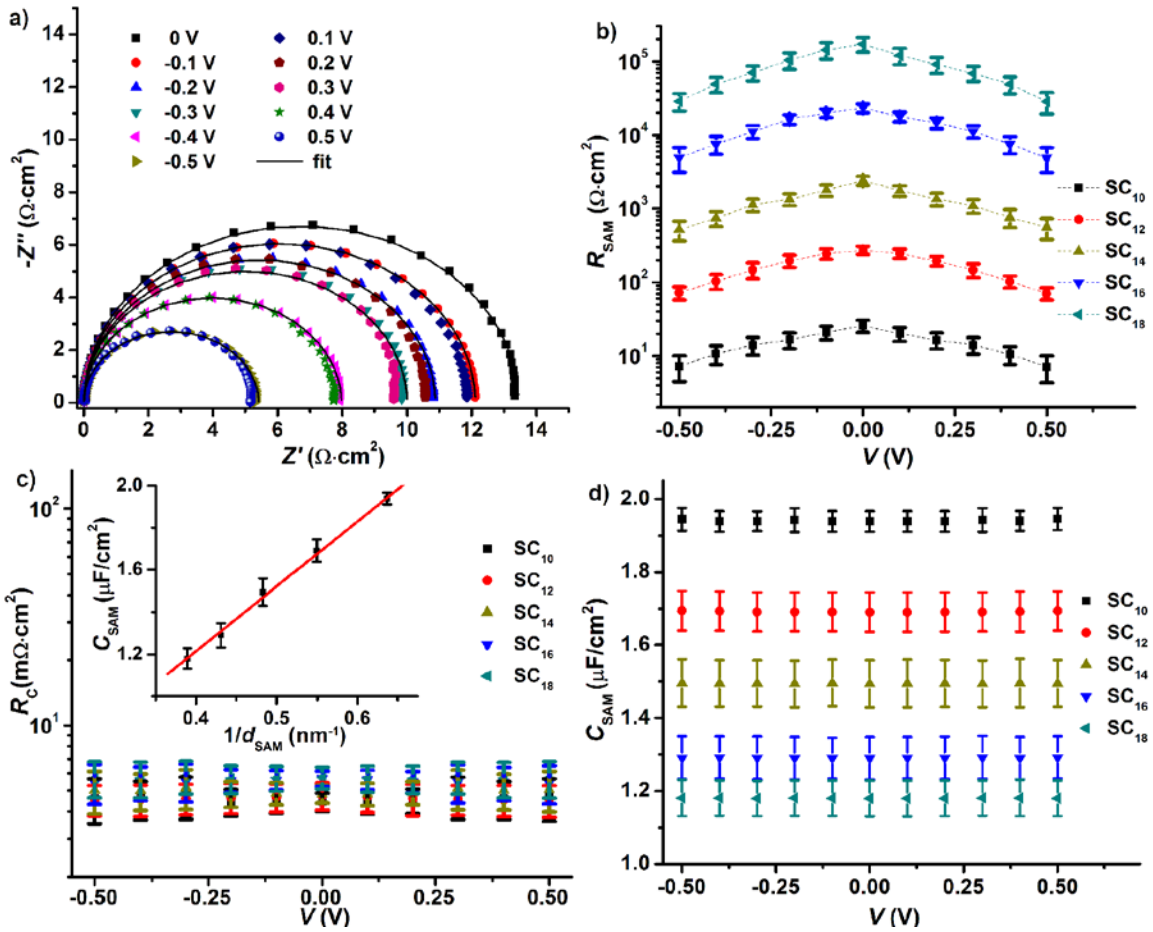

Figure 3: The potentiodynamic impedance data for junctions with SAMs of SC_n (where n = 10, 12, 14, 16 or 18). a) The Nyquist plots for junction with SAMs of SC_{10} as a function of the DC bias. The black solid lines are fits to the equivalent circuit (eqn (2)) shown in Figure 1b. b) A semi-log plot of the value of R_{SAM} vs. DC bias voltage. The dashed lines are guides to the eye. c) The value of R_C vs. DC bias voltage. The inset shows the capacitance of the SAM (C_{SAM}) as a function of $1/d_{SAM}$ and the solid red line is a fit to eqn (5). d) The C_{SAM} as a function of DC bias voltage. The error bars represent the standard deviation of three data sets obtained from three junctions.

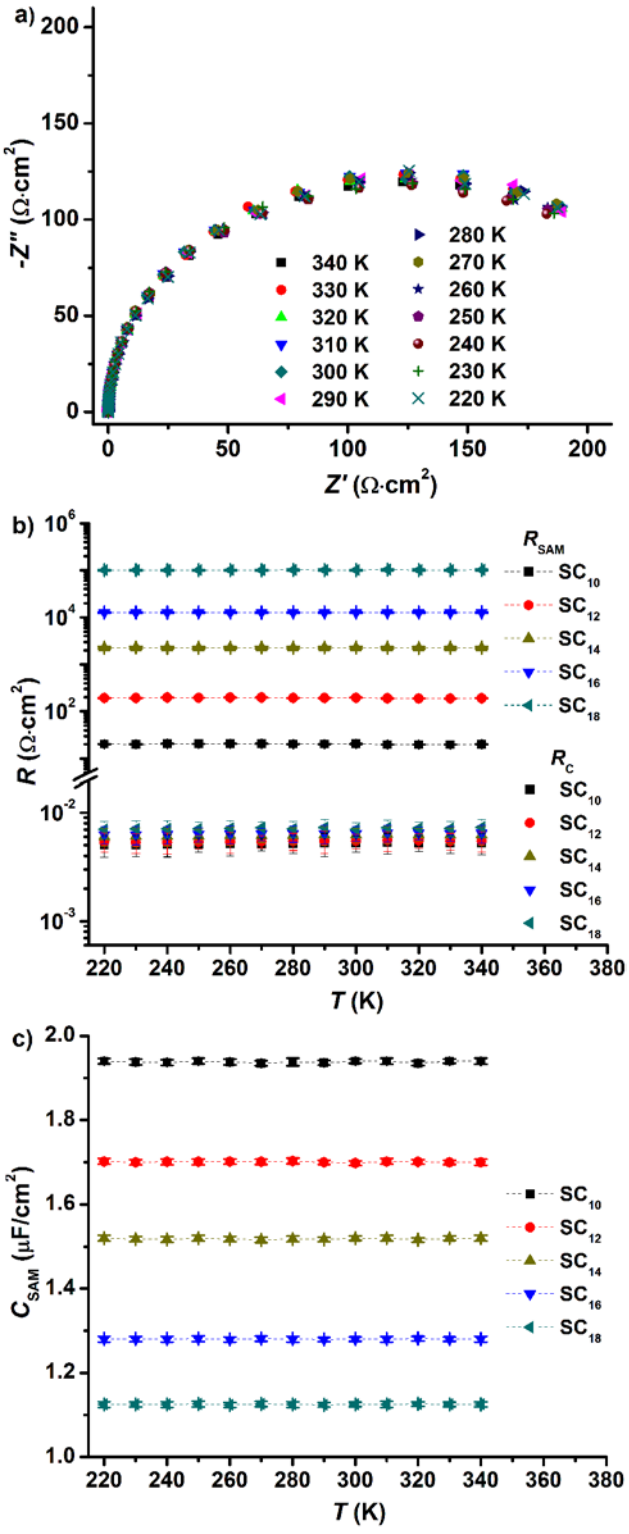

Figure 4: The impedance data at 0 V DC bias as a function of temperature. a) The Nyquist plots for a junction with a SC_{12} SAM measured in the temperature range of 220 – 340 K in steps of 10 K. b) The values of R_{SAM} and R_C vs T. c) The values of C_{SAM} vs T. The error bars represent the error from the fit to the equivalent circuit and the dashed lines are guides to the eye.